NUMERICAL INVESTIGATION OF HELICOPTER MAST-BUMPING SUSCEPTIBILITY IN LOW-G CONDITIONS

Philipp Kunze **Christoph Keßler** **Klausdieter Pahlke**
German Aerospace Center (DLR)
Braunschweig, Germany

ABSTRACT

This paper presents a numerical investigation of helicopter mast-bumping susceptibility in low-G conditions using a comprehensive aeromechanics code. The primary objective of this study is to provide qualitative insights for educational purposes, focusing on the fundamental flight-mechanical effects of helicopters in low-G environments. A key aspect of the research is the comparison between helicopters with zero flapping-hinge offset and hingeless rotors with high flapping stiffness. The study examines the flight-mechanical effects of helicopters during the transition into a low-G dive maneuver, highlighting the influence of the rotor system and different recovery strategies. Furthermore, the influence of flight conditions, such as velocity, and configurational aspects, including stabilizer design, is analyzed. Here, the specific focus is dedicated to the occurring flapping angles, as they directly determine the onset of mast bumping. The findings emphasize the advantages of hingeless rotor systems in low-G conditions, particularly in terms of controllability, and confirm previous results and safety recommendations to mitigate the risk of mast bumping.

NOTATION

*

Symbols

D Drag (N)

I_{xx} Fuselage mass moment of inertia w.r.t. roll axis (kg m^2)

L Helicopter rolling moment (N m)

$L_{\beta_{1s}}$ Lateral flapping stiffness (s^{-2})

M_β First mass moment of rotor blade (kg m)

T Thrust (N)

V Velocity (m s^{-1} or kt)

W Weight (N)

e Non-dimensional flapping-hinge offset (-)

g_0 Standard acceleration of gravity, 9.81 (m s^{-2})

m Helicopter mass (kg)

n_b Number of rotor blades (-)

n_z Load factor (-)

t Time (s)

Δz_{MR} Vertical offset of main rotor from helicopter CG, positive upwards (m)

Φ, Θ, Ψ Helicopter attitude: roll, pitch, yaw (deg)

Ω Rotor angular frequency (rad s^{-1})

α Angle of attack (deg)

$\beta_0, \beta_{1c}, \beta_{1s}$ Flapping angles: coning, longitudinal cyclic, lateral cyclic (deg)

$\theta_0, \theta_{1c}, \theta_{1s}$ Control angles: collective, lateral cyclic, longitudinal cyclic (deg)

ψ Rotor azimuth angle (deg)

*

Acronyms

CG Center of Gravity

DLR German Aerospace Center

ERF European Rotorcraft Forum

FAA Federal Aviation Administration

MR Main Rotor

TR Tail Rotor

TAS True Airspeed

TPP Tip Path Plane

INTRODUCTION

Mast bumping is a well-documented safety concern, particularly for semi-rigid rotor systems. It occurs when the rotor hub contacts the rotor mast due to excessive teetering angles, as depicted in Figure 1. While mild mast bumping may be damped by elastomeric teetering stops, hard mast bumping can cause severe damage to the rotor mast, and even lead to rotor separation from the mast and in-flight breakup of the helicopter. The risk of such fatal accidents is especially elevated during low-G flight conditions accompanied by sudden or large cyclic pilot inputs.

The issue of mast bumping was first identified during the Vietnam War through a series of accidents involving U.S. Army UH-1 and AH-1 helicopters with teetering rotors (Ref. 1). Subsequent investigations by the U.S. Army provided a fundamental understanding of the underlying mechanisms and hazardous flight conditions. This knowledge has been used to train pilots on critical flight conditions to avoid and on recovery strategies when operating teetering rotor helicopters (Ref. 2).

Research has also focused on reducing flapping angles in teetering rotors through simulations: Early studies at Bell Helicopter employed simplified models to examine the effects of hub springs with non-linear spring characteristics on teeter angles (Refs. 3,4). These studies demonstrated that such measures can significantly reduce the risk of mast bumping, particularly during maneuvering flights. More recent studies have investigated low-G mast bumping using advanced simulation tools, focusing on detailed modeling of Robinson helicopter models with tri-hinge rotors (Refs. 5–7), which are known to be susceptible to mast bumping (Ref. 8). These publications also employed simulations to investigate the influence of design parameters, such as blade mass, radial center of gravity location, and horizontal stabilizer orientation, on reducing teeter angles.

Mast bumping is a complex phenomenon that resists simple descriptions, but simulations have proven valuable in understanding its physics and predicting helicopter behavior in unsteady flight conditions. In this study, a comprehensive aeromechanics simulation tool is employed to compare the behavior of a generic helicopter featuring a central flapping hinge rotor to a Bo105 helicopter with a hingeless rotor. The influence of the level of aerodynamic and rotor-dynamic model complexity on simulation results is evaluated. Simulation results are used to describe the mechanisms that make low-G conditions critical for helicopters with zero flapping hinge offset and without hub springs. The effects of various configuration parameters on mast-bumping susceptibility are investigated, and low-G recovery strategies are compared in terms of their effectiveness and resulting flapping angles. This study prioritizes understanding the underlying flight mechanics effects and achieving the necessary level of model complexity to qualitatively simulate the phenomenon, rather than precisely modeling an existing helicopter.

Table 1: Main rotor configuration characteristics: Bo105-mod vs. Bo105-orig.

Characteristic	Bo105-mod	Bo105-orig	Unit
number of blades	2	4	(-)
radius	4.91	4.91	(m)
blade chord	0.54	0.27	(m)
rel. flap hinge offset	0.0	15.2	(%)
Lock number[a]	4.97	8.16	(-)

[a]the Lock number is calculated based on flapping inertia relative to the (virtual) flapping hinge

NUMERICAL MODEL

Numerical simulations are conducted using DLR's multibody aeromechanics comprehensive simulation tool MAECOsim® (Ref. 9), formerly known as VAST. The simulation setup is based on an existing flight mechanics model of the Bo105 helicopter, where airframe, tail surfaces, and rotor blades are represented as rigid bodies in a multibody system. Virtual flap and lag hinges are incorporated into the model in order to capture the fundamental blade dynamics of the hingeless rotor system. The rotor blade aerodynamics are modeled using the blade element method with analytical NACA23012 airfoil polars based on a modified Leiss unsteady airloads formulation (Ref. 10). The main rotor inflow and wake are simulated using the full-span free-wake method described in (Ref. 11). Fuselage, horizontal stabilizer, and fin airloads are evaluated from look-up tables, also taking wind, body motion, and the rotor wake into account. For the tail rotor, the induced velocity components are coupled with the Glauert uniform global inflow model. A weak coupling approach is employed to achieve efficient trim along with the computationally costly free-wake model.

Helicopter Configurations

To investigate the mast bumping issue, a generic helicopter model is derived from a simulation model of the original Bo105 helicopter. The modified model features a two-blade rotor hub with central flapping hinges, as sketched in Figure 8c. This simplified rotor hub representation has shown to deliver similar results as real-world semi-rigid rotor hubs in most regarded cases, as will be shown in the results section.

Figure 2 shows a visual representation of the two helicopter configurations, while modified parameters are listed in Table 1. Following parameters are modified from the original Bo105 model: the number of main rotor blades is reduced to two, while blade chord and mass are doubled, keeping the rotor's radius and solidity constant. Furthermore, flap hinge offsets are set to zero, and virtual lead/lag hinges are removed. The blade mass moments of inertia are adapted according to the modified blade mass, while the radial center of gravity position remains constant. The changes result in a significantly lower Lock number for the modified configuration, corresponding to the value given for a Robinson R22 helicopter in (Ref. 12). Consequently, the predicted flapping

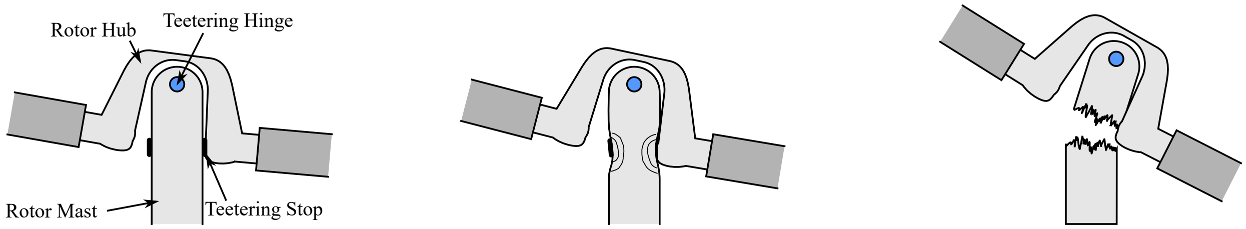

(a) Teetering stop/mast contact

(b) Mast deformation

(c) Rotor separation

Figure 1: Mast damage due to excessive teetering motion shown in different levels of severity.

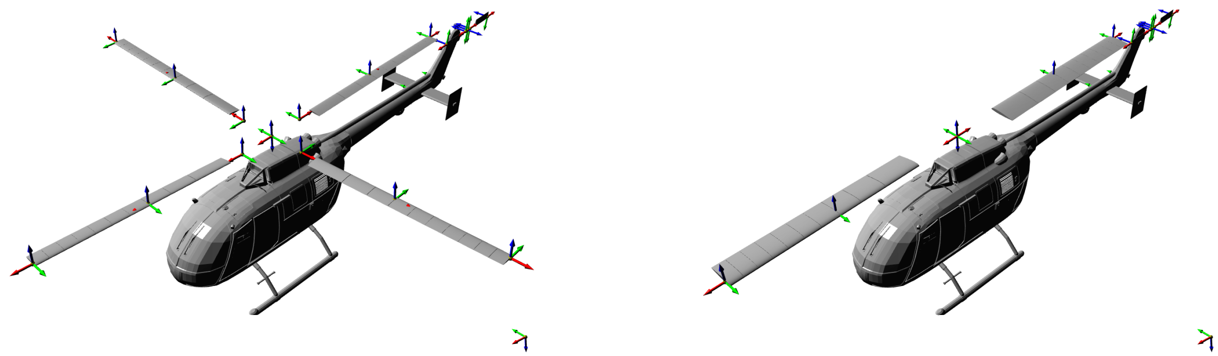

(a) Original Bo105 configuration with virtual flapping and lead-lag hinges (Bo105-orig)

(b) Generic configuration with two-bladed rotor and central flapping hinges (Bo105-mod)

Figure 2: Visual representation of the investigated helicopter configurations in the MAECOsim® GUI.

angles fall within the range of existing semi-rigid rotor helicopters. Further configurational aspects are left unchanged in order to isolate the effect of the rotor system on the flight-mechanical behavior of the helicopters. However, it is important to note that the results may overemphasize some disadvantages of semi-rigid rotors, as real-world designs typically mitigate these issues by adjusting parameters such as vertical offsets of the main and tail rotors from the center of gravity.

RESULTS

This section presents results of the numerical simulations of individual cases:

- Case 1: Push and hold
- Case 2: Push-over
- Case 3: “Bad” recovery
- Case 4: “Good” recovery
- Case 5: Influence of flight velocity
- Case 6: Asymmetrical stabilizer

Unless denoted otherwise, all presented transient simulations start from trimmed level flight at 60 kt. Most cases compare the response of the Bo105-mod configuration to that of the original Bo105 model. The first two cases focus on pilot inputs leading to an unloading of the main rotor and examine the flight-mechanical response of the two configurations during the onset of low-G conditions in detail, also discussing the resulting blade flapping behavior. In addition, for Case 1 the effects of aerodynamic and rotor hub modeling on the simulation results are investigated. The next two cases explore methods for recovering from low-G conditions and incipient high angular rates. Finally, the influence of flight velocity and stabilizer design on helicopter response and blade dynamics is presented.

Case 1: Push and hold

Figure 3 shows transient simulation results for a basic low-G maneuver, for both the generic helicopter configuration and the original Bo105 model. All curves except β_{blade1} show results filtered using a moving average with a period corresponding to one main rotor revolution.

First, the results for the generic Bo105-mod configuration (solid lines) are discussed in detail. The simulation starts from a trimmed level flight at 60 knots. At $t = 1\,\mathrm{s}$, the longitudinal cyclic control is pushed forward by $\Delta\theta_{1s} = -2^\circ$ using a linear ramp of $\Delta t = 0.5\,\mathrm{s}$ duration, and then held fixed at the end position. The corresponding control angles are depicted in the uppermost plot of Figure 3. All other controls are kept constant on the trim value during the complete simulation period

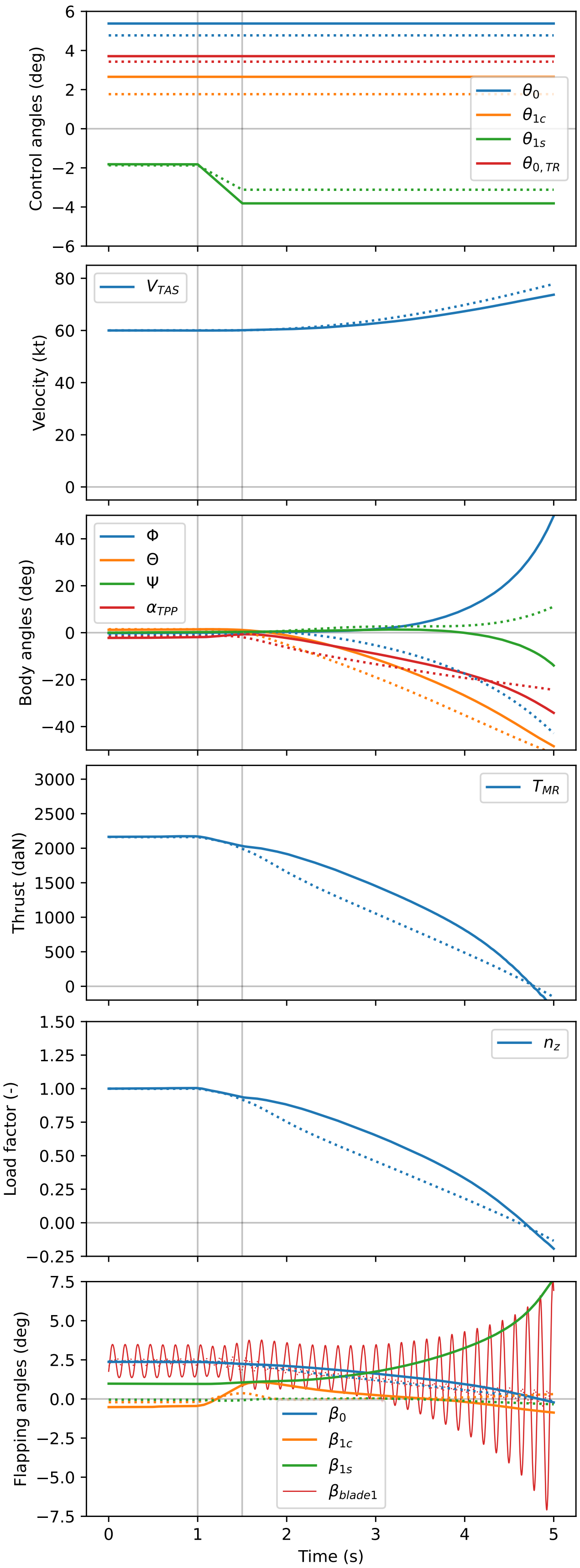

Figure 3: Simulation results for Case 1: Push and hold (—— Bo105-mod, ······ Bo105-orig).

of 5 seconds. The reaction of the helicopter and its blades to the prescribed pilot input is shown on the other plots of the figure.

The Bo105-mod helicopter's response to the pilot's input can be broken down into several key stages. Initially, the input causes the main rotor's tip path plane to tilt forward (β_{1c}, α_{TPP}), resulting in a corresponding rotation of the thrust vector. This generates a moment around the pitch axis, initiating the helicopter's primary response: a pitch-down motion, as illustrated by the Θ curve in Figure 3.

As the helicopter moves forward and pitches down, the rotor disk is increasingly subjected to the freestream from above, reducing the local angle of attack of all blade sections and decreasing the rotor thrust. Consequently, the helicopter starts to lose height, while the true airspeed increases due to the occurring downward acceleration.

The load factor curve closely follows the thrust curve, decreasing rapidly and reaching a value of $n_z = 0.5$ within 2 to 3 seconds after initiating the control input. This rapid unloading of the main rotor significantly contributes to the helicopter's secondary response – an uncommanded roll motion.

As shown in Figure 4 (a) and (b), the tail rotor thrust counters the main rotor torque in the trimmed state, while the main rotor disk is slightly tilted to the left to compensate for the tail rotor thrust. However, during the maneuver, the main rotor is unloaded rapidly, reducing its thrust while the tail rotor thrust remains approximately constant due to the fixed pedal position. Consequently, the roll moment generated by the main rotor diminishes, while the roll moment generated by the tail rotor remains constant, causing an increase in the roll rate to the right (starboard side). By the end of the simulation, 4 seconds after initiating the pilot input, the uncommanded right roll reaches the same order of magnitude as the primary pitch-down response.

The reduction in the coning angle (β_0) also indicates that the main rotor load is progressively relieved. Here, the cyclic flapping angle coefficients are decisive for the risk of mast bumping. The flapping angle plot axis limits are set to ± 7.5 deg, consistent with typical flapping clearances in semi-rigid rotor designs at teeter stop engagement. Mast bumping is expected when the cyclic flapping amplitude $\sqrt{\beta_{1c}^2 + \beta_{1s}^2}$ exceeds this threshold. In this simulation, the longitudinal flapping (β_{1c}) decreases after the longitudinal input ramp finishes, while the lateral flapping (β_{1s}) is continuously amplified with the onset of the rolling motion, as sketched in Figure 4 (b) and (c). Thus, mast bumping is expected toward the end of the simulation.

In the primary response, the observed behavior of the Bo105-orig (dotted lines in Figure 3) configuration resembles that of the modified Bo105-mod (solid lines Figure 3) configuration described above. Both helicopters exhibit similar behavior, i.e. tilting forward and accelerating as main rotor thrust decreases due to increased flow through the rotor disk. However, a closer examination of the Bo105-orig curves reveals a nearly linear progression in pitch angle, thrust, and load factor

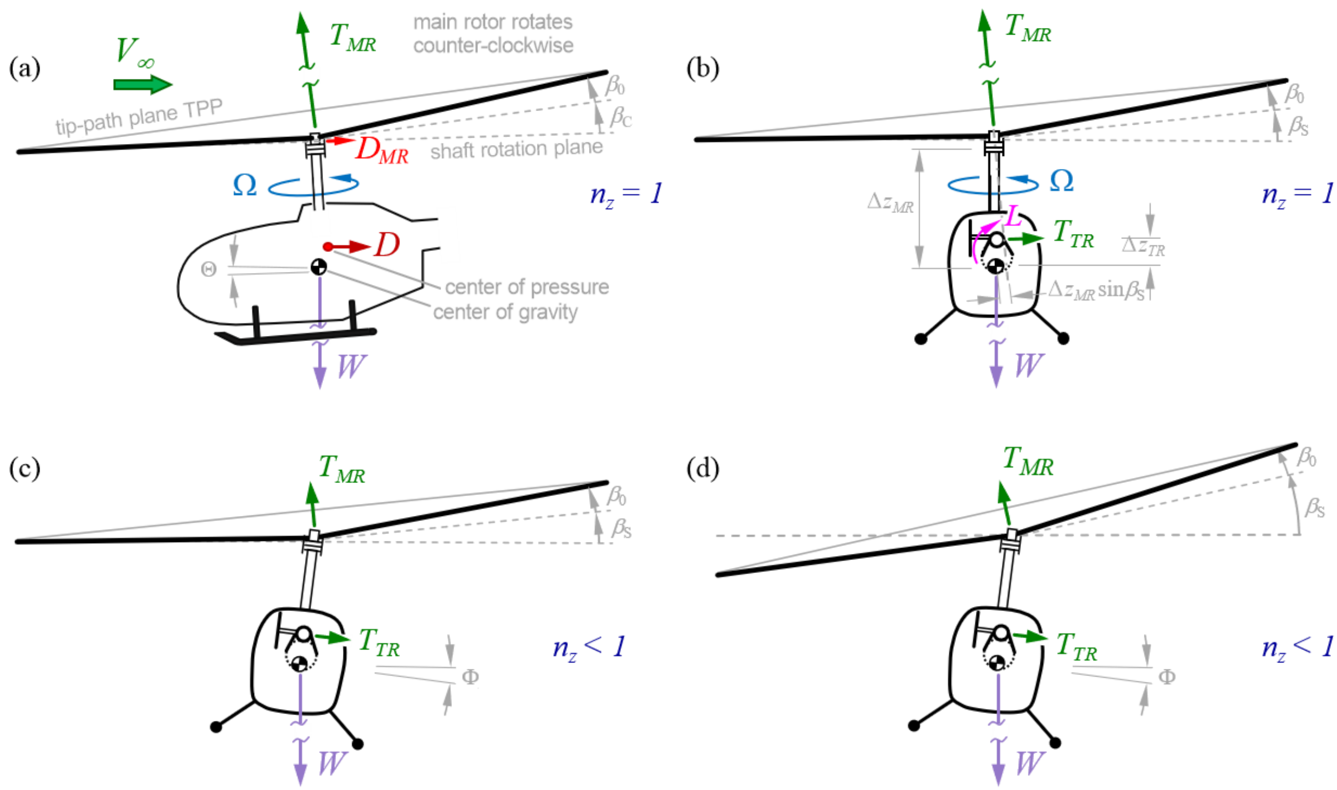

Figure 4: Illustration of primary flight mechanical effects resulting from a negative longitudinal cyclic ramp input (push) applied to the generic Bo105-mod helicopter in trimmed level flight conditions ((a): side view, (b)-(d): rear view).

subsequent to the input ramp. Note that a smaller longitudinal cyclic control input is used for Bo105-orig ($\Delta\theta_{1s} = -1.25°$) compared to Bo105-mod ($\Delta\theta_{1s} = -2.00°$) to account for the higher responsivity of its hingeless rotor system. This adjustment ensures a comparable timeframe for an entire unloading of the main rotor ($T_{MR} = 0\,\text{N}$) in both configurations. In contrast, the secondary response of the two helicopters reveals notable differences. Although the rates of uncommanded roll motion and yaw motion onset are similar, their directions are opposite. Specifically, Bo105-mod rolls right and yaws left, whereas Bo105-orig rolls left and yaws right. This response difference is visualized in Figure 5, which shows the distinct attitudes of the two configurations at $t = 3.5\,\text{s}$.

Figure 6 illustrates the component-wise roll moment contributions w.r.t. the center of gravity for both configurations, including aerodynamic and inertial loads. In the trimmed state, the main rotor roll moment primarily counteracts the roll moment generated by the tail rotor for both configurations. However, Bo105-orig main and tail rotor produce approximately 15 % less roll moment than that of Bo105-mod. During the cyclic input ramp, the main rotor roll moment contribution of the Bo105-mod configuration remains relatively constant, only gradually weakening as the main rotor loading decreases. In contrast, the Bo105-orig's main rotor roll moment contribution changes significantly already during the cyclic input ramp. First, its absolute value decreases for approximately 0.25 seconds, then starts increasing until reaching a plateau within the following 0.25 seconds after the end of the ramp, resulting in a considerable offset (approximately $-300\,\text{Nm}$) from the trimmed value. This leads to a negative total rolling moment, causing an accelerated rolling motion to the left. Although the aforementioned roll moment contribution by the main rotor reduces as its thrust breaks down near $t = 3$ seconds, the resulting roll moment remains negative until the end of the simulation. This is attributed to the fact that the tail rotor's rightwards rolling moment contribution also decreases due to the changes in the helicopter's attitude and motion, which reduce the effective angle of attack of the tail rotor.

The discrepancies in rolling moment contribution can be explained by differences in the rotor systems, primarily modeled by the (virtual) flapping hinge offset. The original Bo105 main rotor, with its stiff blade attachment, exhibits a high moment capacity. In contrast, the modified main rotor, featuring central flapping hinges, has a negligible moment capacity. The rolling moment contribution of the main rotor can be approximated by a linear flapping spring (Ref. 13)

$$L \approx I_{xx} L_{\beta_{1s}} \beta_{1s} \tag{1}$$

where the lateral flapping stiffness $L_{\beta_{1s}}$ can be estimated as (Ref. 13)

$$-L_{\beta_{1s}} \approx \frac{W \Delta z_{MR}}{I_{xx}} + \frac{n_b M_\beta \Omega^2 e}{2 I_{xx}} \tag{2}$$

The primary contribution to the lateral rotor flapping stiffness in the original hingeless Bo105-orig configuration arises from

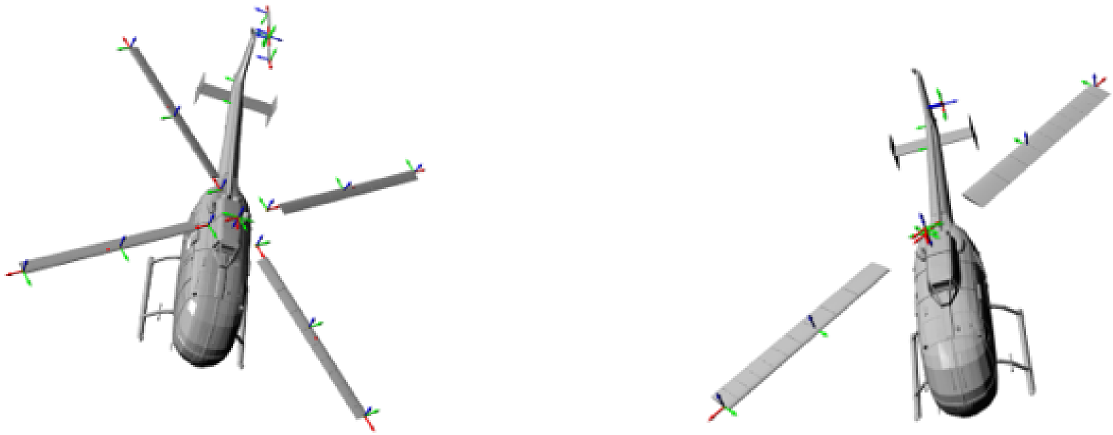

(a) Bo105-orig (b) Bo105-mod

Figure 5: Case 1: Front view snapshot of the two investigated rotorcraft configurations at $t = 3.5\,\mathrm{s}$, illustrating the contrasting uncommanded roll and yaw behaviors.

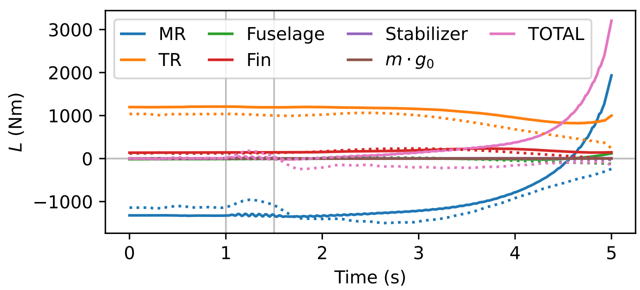

Figure 6: Case 1: Componentwise roll moment contributions (—— Bo105-mod, ······ Bo105-orig).

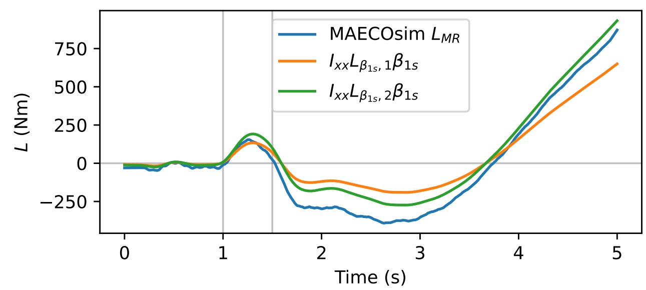

Figure 7: Case 1: Comparison between estimated main rotor roll moment contribution from linear flapping stiffness and MAECOsim® result for Bo105-orig vs. simulated time.

the virtual flap hinge offset e that affects the second term in Equation 2. A secondary contribution comes from the vertical offset of the main rotor from the center of gravity, captured by the first term in Equation 2. In the modified Bo105-mod configuration, the flapping hinge offset is zero, eliminating the second term's contribution. Figure 7 presents a comparison of the main rotor rolling moment contribution for the Bo105-orig configuration, contrasting the analytical approximation using a linear flapping spring model with the results from the numerical simulation conducted in MAECOsim®. $L_{\beta_{1s},1} = -89.4\,\mathrm{s}^{-2}$ is estimated using the relations given above, while $L_{\beta_{1s},2} = -128.2\,\mathrm{s}^{-2}$ is determined using linear least-squares approximation. The clearly observable correlation between large sections of the curves indicates that this first-order term is a primary contributor to the main rotor rolling moment for the Bo105-orig configuration. Conversely, the modified rotor system of the Bo105-mod configuration is unable to produce notable hub moments, with the estimated flapping stiffness being only approximately 20 % that of the Bo105-orig rotor.

The distinct rotor systems are also evident in the resulting flapping angles, as shown in the last plot of Figure 3. The original Bo105-orig configuration exhibits significantly smaller cyclic flapping angles due to its high moment capacity. Notable longitudinal flapping angles are only observed during the cyclic input ramp and shortly thereafter, which corresponds to the period when the fuselage attitude adjusts to the commanded rotation of the rotor's tip-path plane. The lateral flapping angles are even smaller and only become noticeable towards the end of the simulation, as the helicopter develops a high roll rate.

Influence of aerodynamics and rotor dynamics modeling Prior to conducting further mast-bumping investigations, Case 1 was utilized to examine the influence of different modeling settings on the simulation results. The key findings and results of this study are presented below.

Firstly, simulations were conducted using both the full-span free-wake model and the Pitt and Peters dynamic inflow model. Although results are omitted for brevity, both models predict nearly identical trends for global flight mechanics and rotor blade dynamics in this case, despite differences in modeling fidelity. However, this agreement is case-specific and not generalizable. Thus, the higher-fidelity free-wake model is used for all simulations reported herein.

The influence of unsteady aerodynamics was also assessed by performing a simulation with the unsteady terms of the analytical Leiss model disabled (results not shown). At the moderate forward speed of 60 kt (advance ratio $\mu = 0.14$), unsteady effects have negligible impact on the results. Nevertheless, unsteady airload terms are retained in all simulations, as they improve accuracy with minimal computational overhead.

Finally, the influence of different rotor hub models on the simulation results was investigated. Figure 8 sketches typical semi-rigid rotor hub designs by Robinson (Figure 8a) and Bell (Figure 8b) together with an idealized rotor hub configuration with two individual central flapping hinges (Figure 8c), which has been used for first investigations on mast bumping at DLR based on a legacy comprehensive helicopter simulation tool. The flexible MAECOsim® multi-body system approach enables straightforward modeling of various rotor hubs. To assess the impact on results, simulations were conducted with different hub types. Figure 9 presents a comparison of exemplary BO105-mod results between the simplified rotor hub and a Bell-type teetering hub with a 2.5° fixed precone angle and 0.08 m underslung. The differing degrees of freedom have a negligible impact on the observed variables. The offset in flapping angles arises because the precone angle of the teetering rotor is not accounted for, whereas the individual flapping hinges allow for natural adjustment of the coning angle β_0 based on rotor load. Thus, the slight divergence observed in the results when rotor loading is significantly reduced is expected. It primarily affects the uncommanded roll motion, which grows slightly faster for the teetering hub, and is also reflected in the lateral flapping angles. However, these minor quantitative differences do not impact qualitative results. A Robinson-type configuration with similar underslung was also simulated in MAECOsim®, yielding results that closely matched the simplified hub. Given the focus on qualitative results and the chance for verification with existing legacy simulations, the simplified configuration was retained for this study.

Case 2: Push-over

Several numerical simulation studies (Refs. 6,7) initiated low-G conditions through a push-over maneuver to predict mast bumping. This maneuver involves a brief pull of the longitudinal cyclic stick followed by a push forward of larger magnitude. To investigate the effect of this maneuver on helicopter response and flapping angles, the pilot controls from the baseline simulation (Case 1) are modified for Case 2.

The adapted pilot controls and corresponding simulation results are shown in Figure 10. The initial longitudinal pull command begins at $t = 0$ and employs an identical magnitude ($\Delta\theta_{1s} = 2°$ for Bo105-mod) and ramp duration as the push command in Case 1. Immediately thereafter, a longitudinal push command is initiated with a magnitude and duration twice that of the initial pull, ending at $t = 1.5$ s, exactly at the same time and longitudinal control angle as the pilot input for Case 1. Starting from $t = 1$ s, the flight-mechanical responses exhibit qualitatively very similar results to Case 1. Notably, the effect of pushing the stick is delayed due to the initial pitch-up motion enforced at the beginning of the maneuver. As a result, the helicopter's pitch attitude achieves a higher value by the time the push command takes effect, and the flight velocity increases at a lower rate. This also delays the coupled uncommanded roll motion. Consequently, the rotors of both configurations remain partially loaded at the end of the simulation for Case 2. The flapping angles in this case exhibit similar behavior to Case 1 but with significantly reduced amplitude at the end of the maneuver, correlating with the roll attitude.

In conclusion, the qualitative effects observed in Case 1 and Case 2 are similar. However, the simulation time and computational effort required to achieve a given $n_z < 1$ are reduced when using the pilot input sequence from Case 1. Therefore, this input sequence is adopted for all subsequent cases to initiate low-G conditions.

Case 3: "Bad" recovery

Cases 3 and 4 are initiated with the pilot input sequence of Case 1, but subsequently demonstrate recovery strategies to counteract the uncommanded roll, commencing at $t = 3$s.

A natural pilot response to counteract the uncommanded roll motion of the helicopter might be to apply a pure lateral cyclic input in the opposite sense. This strategy is investigated in Case 3. However, for helicopters featuring central flapping hinges, this approach is rendered ineffective when the main rotor thrust is substantially reduced, as the lateral control authority is severely compromised due to the rotor's diminished moment-generating capacity. Although the supplementary aerodynamic loads induced by cyclic pitch remain effective in tilting the rotor disk, the diminished thrust renders the lateral cyclic input insufficient to counteract the roll motion. In this scenario, the pilot may instinctively increase the countering lateral cyclic input, but this may lead to critical flapping angles and exacerbate the mast-bumping risk without generating sufficient moment to counter the roll. As emphasized in (Ref. 14), it is crucial to avoid this recovery strategy.

Figure 11 shows the control inputs and simulation results for Case 3. The initial longitudinal cyclic input corresponds to Case 1, until at $t = 3$ s, a lateral cyclic control angle ramp of the same amplitude as the initial longitudinal cyclic ramp is initiated in order to counter the uncommanded roll motion. Thus, the sign of the recovery input is opposite for the two configurations: positive for Bo105-mod and negative for Bo105-orig. In the case of Bo105-mod (solid lines), the recovery input starts when the load factor reaches approximately $n_z \approx 0.6$. Nevertheless, the control is not sufficient to significantly slow down the rolling motion. The increase of the roll rate is slightly delayed when compared to Case 1. But the pitch-down motion is not affected, thus the thrust decay continues, reducing the control authority and the efficiency of the recovery input. The timeframe of complete rotor unloading is not changed remarkably by the recovery. However, the lateral flapping closely follows the lateral cyclic input ramp, augmenting the flapping amplitude from ca. 1° to ca. 4°.

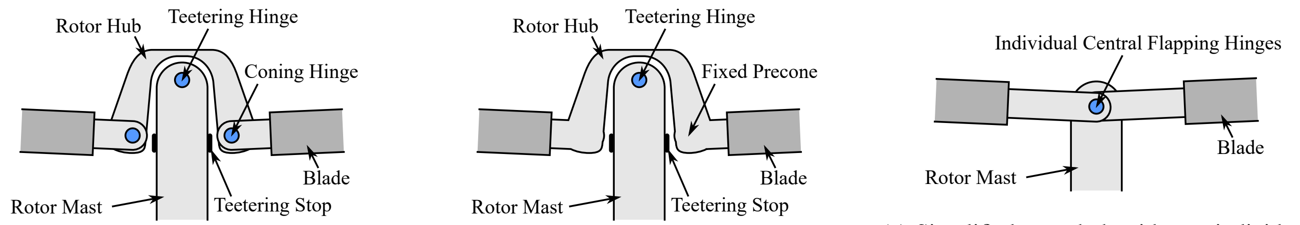

(a) Robinson-type tri-hinge rotor hub

(b) Bell-type teetering rotor hub

(c) Simplified rotor hub with two individual central flapping hinges

Figure 8: Modeled rotor hubs

The simulation confirms that pure lateral cyclic input is ineffective for countering the uncommanded roll motion and recovering from the low-G conditions. Larger lateral inputs may even lead to critical flapping angles, without restoring control authority. Reversing the pitch-down movement is crucial for re-loading the rotor and re-gaining the full control authority.

In contrast, the Bo105-orig configuration (dotted lines) demonstrates that the control authority remains largely uncompromised in low-G conditions. The roll angle stabilizes rapidly after countersteering, despite a significant reduction in rotor load at the onset of recovery input ($n_z(t = 3\,\mathrm{s}) \approx 0.3$) compared to the Bo105-mod configuration. This highlights a key advantage of articulated rotor systems: maintaining agility and control effectiveness in low-G conditions. Furthermore, the hingeless rotor system exhibits flapping angles at an order of magnitude smaller than the rotor with central flapping hinges, enabling reduced clearance between the rotor and surrounding components and thus more flexibility in the helicopter design.

Case 4: ”Good” recovery

The low-G recovery recommended in a Safety Notice by the Robinson Helicopter Company (Ref. 14) involves reloading the rotor by gently pulling longitudinal cyclic to recover thrust and control authority, followed by stopping the roll with lateral cyclic. Simulation Case 4 strives to implement this recovery procedure. The results are depicted in Figure 12. The total simulation time for Case 4 is extended to 9 s to fully capture the recovery process.

Similar to Case 3, the recovery input begins 3 seconds into the simulation, 2 seconds after inducing low-G conditions by pushing the cyclic stick forward. At this point, the load factor decreases significantly, to $n_z \approx 0.6$ for the Bo105-mod configuration and $n_z \approx 0.3$ for the Bo105-orig configuration.

The recovery maneuver is initiated by pulling the cyclic stick back through a 0.5 s ramp, followed by a 1-second hold at the resulting position, and then returning to an approximately trimmed position through another 0.5 s ramp. Following the longitudinal cyclic input, a 0.5 s lateral cyclic ramp is applied and held for approximately 1 second, before being terminated with another 0.5 s ramp, resulting in a trimmed state. The input amplitudes and lateral hold duration are manually optimized to achieve a trimmed state with constant velocity and near-zero attitude angles by the end of the maneuver, while avoiding excessive flapping angles for the Bo105-mod configuration. As a result, both configurations stabilize at a flight speed of approximately 80 kt with near-zero pitch and roll angles. However, the yaw angles remain between 15° to 20° (positive yaw for Bo105-mod, negative yaw for Bo105-orig) due to the absence of pedal input to counter the uncommanded yaw during the maneuver.

The simulation of the Bo105-mod configuration demonstrates the feasibility of achieving a successful recovery using this approach. The longitudinal cyclic input initiated at $t = 3\,\mathrm{s}$ primarily recovers the main rotor thrust. Furthermore, the subsequent lateral cyclic roll recovery input contributes an additional, nearly equal amount to the thrust recovery, attributed to roll-pitch coupling effects. Notably, the commanded roll following pitch recovery is effective, indicating a regained cyclic control authority. This is further illustrated by the angle-of-attack distributions in Figure 13. Compared to the trimmed condition (Figure 13a), the angles of attack at $t \approx 2.5\,\mathrm{s}$, shortly before the recovery is initiated, are significantly reduced (Figure 13b). By the end of the longitudinal recovery input, the original angle-of-attack levels are largely restored (Figure 13c).

Nevertheless, applying longitudinal input in forward flight results with large longitudinal flapping angles, which are necessary to recover the main rotor thrust. Additional simulations showed that gentler longitudinal inputs are insufficient to fully recover the initial pitch attitude for the Bo105-mod configuration. Additionally, initiating a delayed recovery command (e.g. at $t = 3.5\,\mathrm{s}$) proves almost impossible to recover without experiencing excessive flapping angles and potential mast bumping, despite the load factor at the start of recovery ($n_z \approx 0.5$) still being significantly greater than zero. This highlights the necessity of quick reaction when encountering low-G conditions with a zero-flapping-offset rotor. If the recovery is delayed too long, a “point of no return” may be reached, beyond which a recovery without the risk of severe mast bumping is inevitable.

In contrast, the original hingeless Bo105 rotor configuration retains cyclic control authority in low-G conditions due to its inherent moment-generating capacity, thereby enabling a

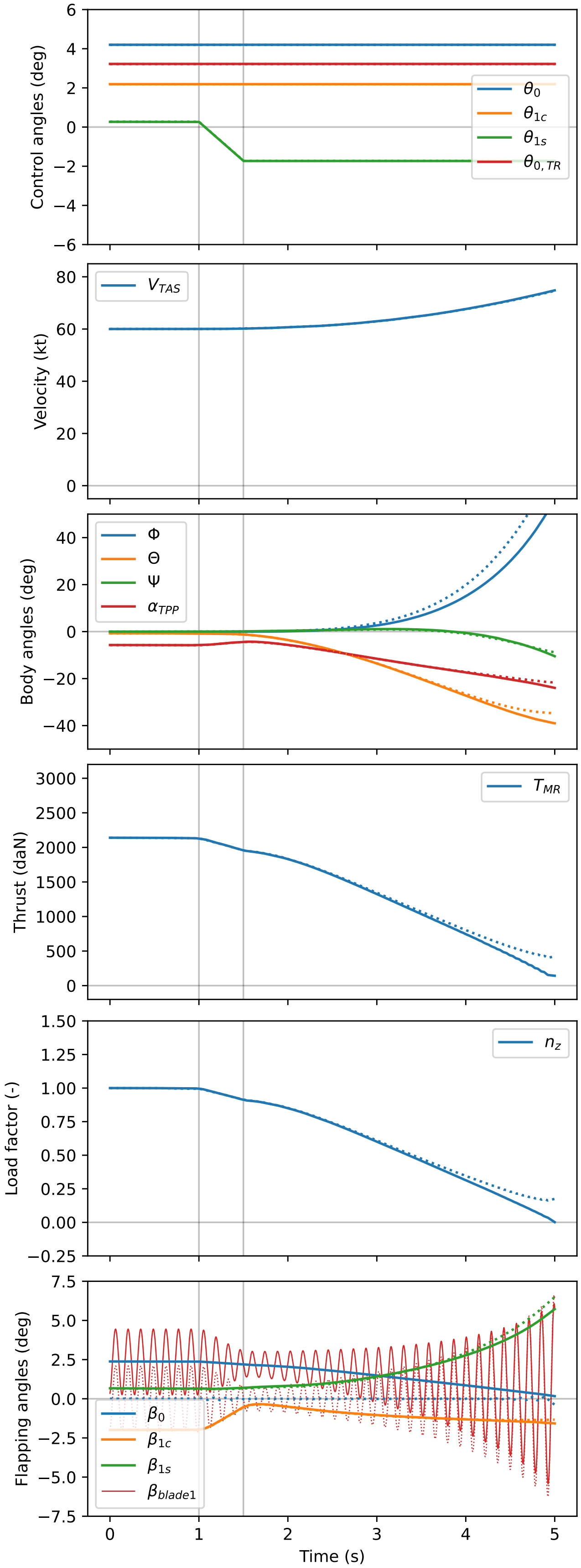

Figure 9: Simulation results for Case 1: Push and hold, Bo105-mod (—— simplified hub, ······ teetering hub).

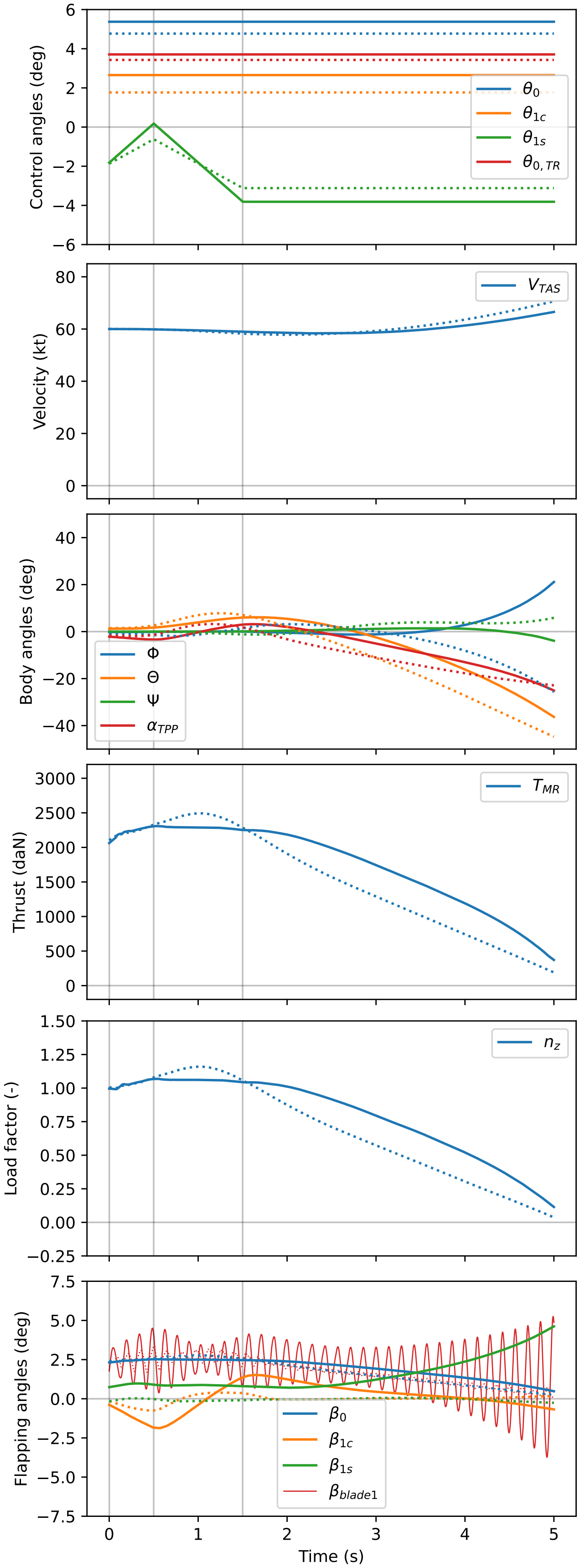

Figure 10: Simulation results for Case 2: Push-over (—— Bo105-mod, ······ Bo105-orig).

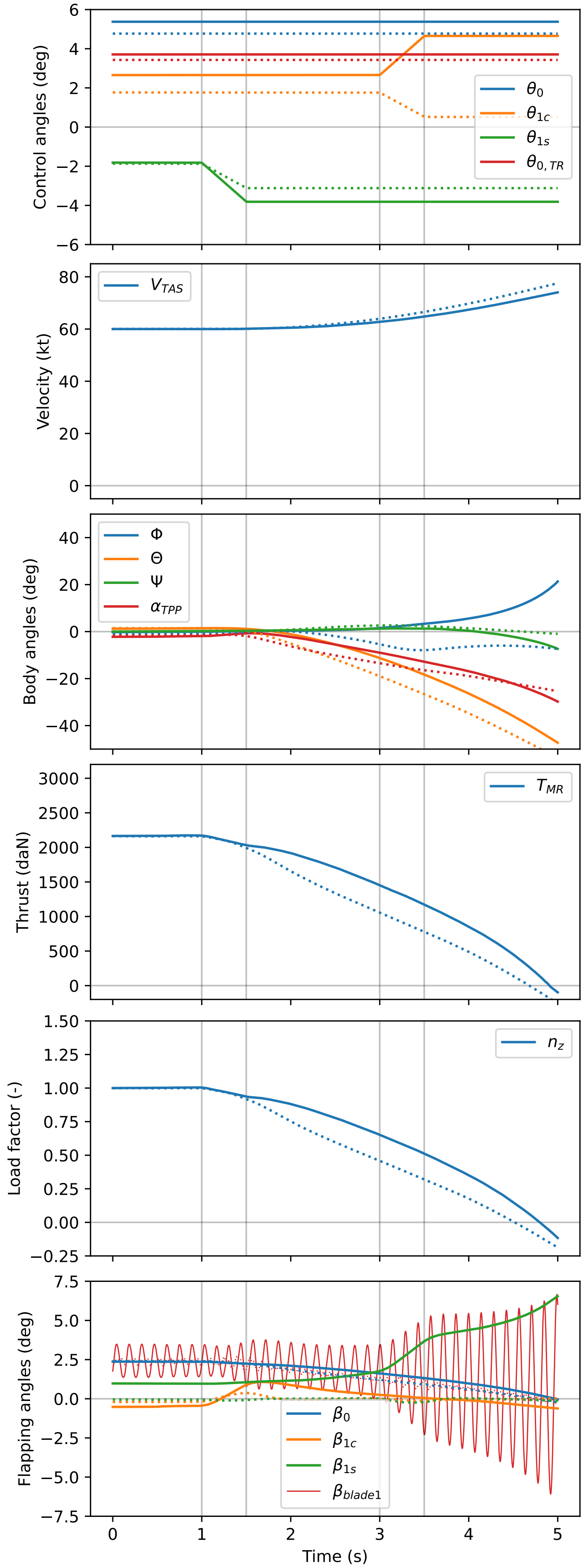

Figure 11: Simulation results for Case 3: Push and "bad" recovery (—— Bo105-mod, ······ Bo105-orig).

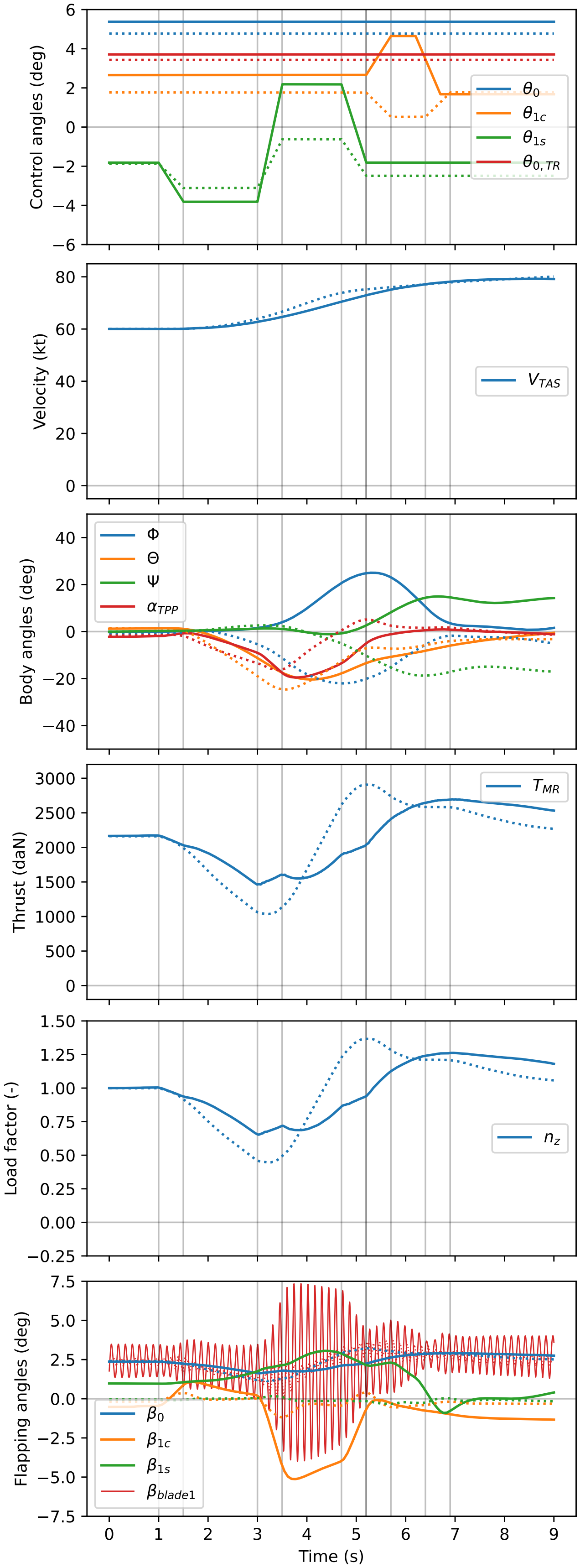

Figure 12: Simulation results for Case 4: Push and "good" recovery (—— Bo105-mod, ······ Bo105-orig).

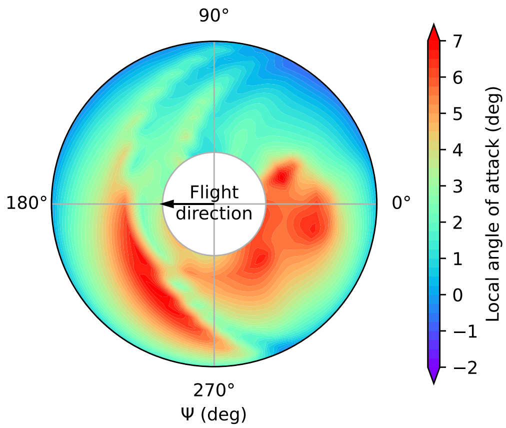

(a) 1st revolution ($t = 0.000 \ldots 0.142$ s)

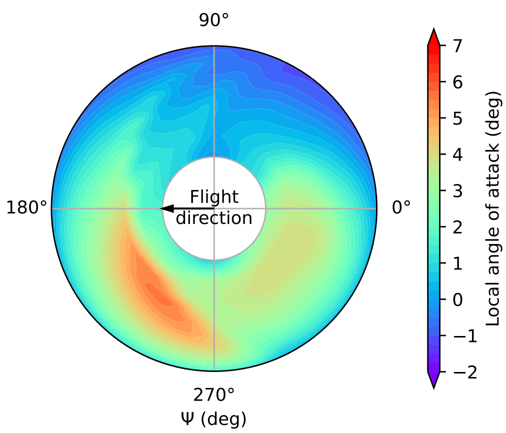

(b) 21st revolution ($t = 2.830 \ldots 2.972$ s)

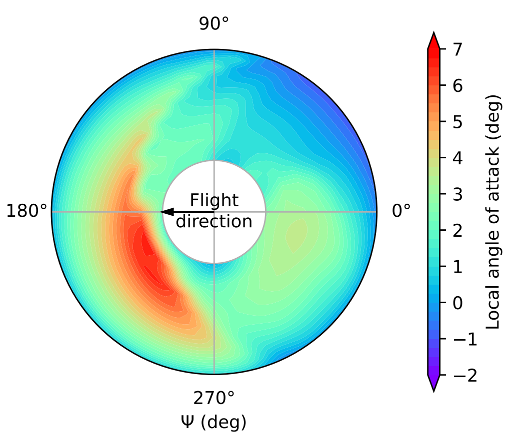

(c) 33rd revolution ($t = 4.528 \ldots 4.670$ s)

Figure 13: Local angle of attack distributions for three different main rotor revolutions in the course of the Case 4 simulation for Bo105-mod.

straightforward recovery with a substantially reduced level of blade flapping.

Case 5: Influence of flight velocity (60 kt vs. 100 kt)

A widely recommended approach to mitigate the risk of mast bumping, as noted in another Robinson Helicopter Safety notice (Ref. 15), is to reduce cruise speed to below 60 kt to 70 kt, particularly in turbulent or potentially turbulent conditions. To investigate the impact of higher velocity on the helicopter's response and flapping behavior, Case 3 ("bad" recovery) is rerun starting from trimmed level flight at 100 kt, corresponding to an advance ratio of $\mu = 0.24$. The results for this higher initial velocity are presented in Figure 14. The axis limits are kept identical as for all previous cases, therefore individual curves are clipped. Nevertheless, clipping only occurs in regions which are beyond the validity range of the engaged models and which are not in the focus of this investigation.

Identical control input produces a response with higher angular rates, corresponding with the increased velocity. Hence, the main rotor thrust decays at a higher rate. Notably, for the Bo105-orig configuration, the rotor becomes completely unloaded approximately 1.5 s after the longitudinal pilot input begins. Despite this, the lateral cyclic remains effective, even at negative load factor, when countering the uncommanded roll. In contrast, the Bo105-mod configuration requires approximately 2.5 s for the main rotor to become completely unloaded upon commencing the longitudinal input. However, the accelerated uncommanded roll motion is largely unaffected by the opposing recovery input initiated through $theta_{1c}$ at $t = 3$ s, and the lateral flapping is rapidly amplified by the onset of the roll motion, leading to a roll attitude exceeding 90° just 3 seconds after initiating the maneuver by longitudinal pilot input ($theta_{1s}$).

The simulation results show that higher flight velocities increase the sensitivity of the rotorcraft response to control inputs and result in increased longitudinal flapping in trimmed flight. Consequently, the pilot's reaction time to vertical gusts with equal relative velocity is reduced, and the margin for maximum flapping angles is also decreased. These factors collectively increase the risk of mast bumping and underscore the validity of the advice given in Robinson's safety notice (Ref. 15).

Case 6: Asymmetrical stabilizer

Lastly, the impact of the horizontal stabilizer configuration on the onset of and recovery from low-G conditions is examined. As described in (Ref. 16), Robinson has introduced new symmetrical horizontal stabilizer designs for their R22, R44, and R66 helicopter models, which aim to mitigate the right-rolling tendency that occurs when operating outside the approved flight envelope. The original stabilizer features an asymmetrical design, extending only to the starboard side, opposite the tail rotor. The new stabilizer design is expected to

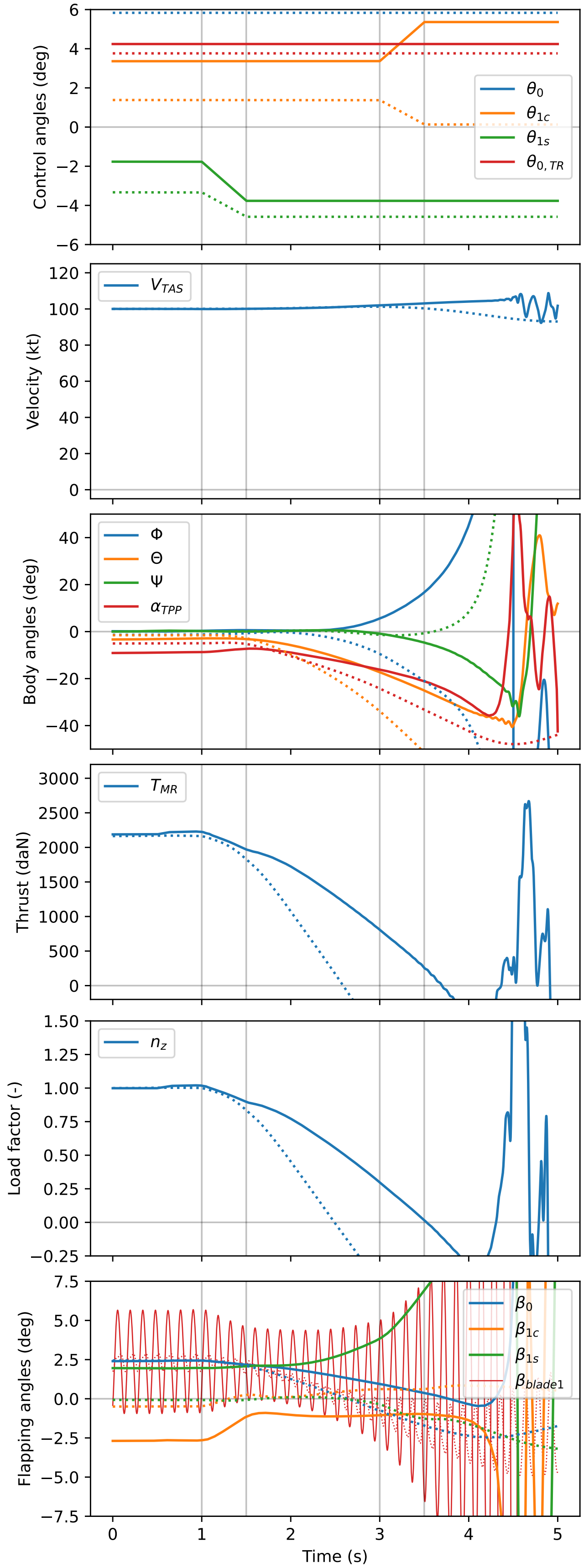

Figure 14: Simulation results for Case 5: "Bad" recovery at 100 kt (—— Bo105-mod, ······· Bo105-orig).

reduce the helicopter's uncommanded roll tendency, mitigating the mast bumping risk by minimizing the cyclic inputs required to recover from unintended roll motion.

The original Bo105 configuration investigated in this paper features a symmetrical horizontal stabilizer design, which is also adopted for the modified Bo105-mod configuration. To examine the effects of an asymmetric stabilizer design, the aerodynamic center of the stabilizer is shifted from the symmetry plane to the estimated center of pressure of the Robinson R44 tailplane, located on the starboard side.

Simulation results for both symmetrical and asymmetrical stabilizer configurations are shown in Figure 15, using the baseline pilot inputs from Case 1. Compared to the symmetrical configuration (solid lines), the asymmetrical configuration (dotted lines) exhibits a significantly higher uncommanded roll rate, resulting in an approximately 66 % greater roll angle at the end of the simulation. Likewise, the lateral flapping angles increase in the asymmetrical configuration, while all other simulation parameters show only minor differences between the two configurations.

The increased roll rate in the asymmetrical configuration results from the helicopter's pitch-down motion, which reduces the stabilizer's angle of attack and consequently increases the downforce acting at its aerodynamic center. In the symmetrical design, the stabilizer downforce produces no moment about the roll axis due to its lateral alignment with the axis. In contrast, the asymmetrical stabilizer's downforce acts with a lateral offset from the roll axis, creating a moment arm that induces a rightward roll moment, augmenting the existing rightward roll moment generated by the tail rotor.

Overall, the asymmetric stabilizer amplifies the uncommanded roll motion. For the symmetric configuration on the other hand, the roll in the same direction caused by the tail rotor remains critical. Nevertheless, it is worthwhile to mention that the vertical tail rotor offset in the Bo105-based configurations studied is not representative for helicopter designs with semi-rigid rotor systems, which typically feature smaller offsets. Consequently, for helicopters like Robinson models, the tail rotor's rolling moment contribution is significantly reduced, making the asymmetric elevator's contribution even more pronounced.

CONCLUSIONS

The primary conclusions of this study can be summarized as follows:

1. A simplified generic helicopter configuration with central flapping hinges based on the Bo105 helicopter was modeled in DLR's comprehensive aeromechanics simulation tool MAECOsim® for investigating the basic flight-mechanical effects of helicopters with different rotor systems in low-G conditions. The focus was on qualitative results mainly for educational purposes (i.e. lecture material).

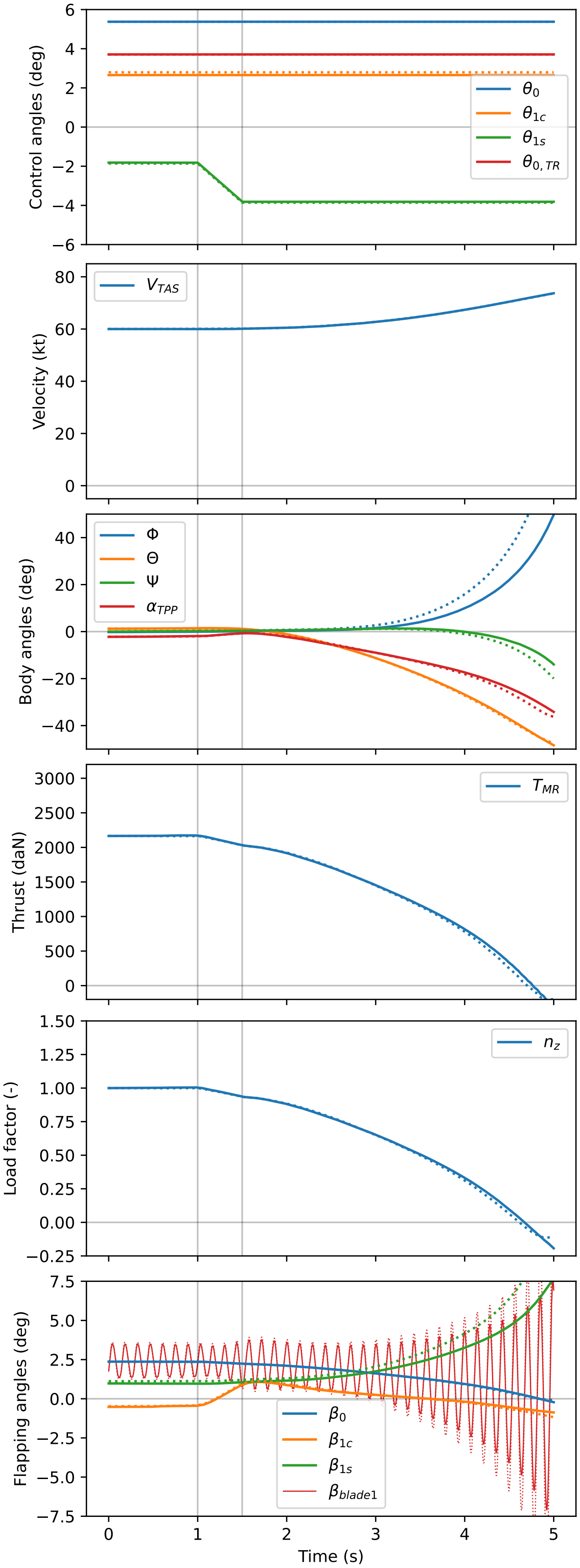

Figure 15: Simulation results for Case 6: Bo105-mod stabilizer configuration (—— symmetrical, ······ asymmetrical).

2. First, the influence of aerodynamic modeling (Pitt and Peters dynamic inflow vs. free-wake, steady vs. unsteady aerodynamics) and rotor-dynamic modeling (e.g. teetering rotor vs. individual flapping hinges) on low-G maneuver results was examined. The analysis revealed that these factors have a minor impact on the results of the regarded case, primarily due to the timeframe of the maneuver being much larger than the main rotor rotation period and rapid convection of the wake away from the rotor blades in forward flight.

3. An analysis of the low-G mast bumping phenomenon was conducted, comparing the flight mechanical responses and flapping dynamics of helicopters with hingeless rotor systems and those with zero flapping-hinge offset.

4. The study reproduced basic observations from previous numerical studies and safety recommendations regarding mast-bumping susceptibility in low-G conditions.

5. Simulation results showed the effects of different recovery techniques, flight states (velocity) and configuration parameters (stabilizer design) on low-G behavior and flapping angles. The results confirmed that higher velocities increase flapping angles and reduce the pilot's time for reaction, thereby increasing the risk of mast bumping. An asymmetrical stabilizer design was also found to amplify uncommanded roll, reducing the timeframe for effective recovery.

It is essential to note that the generic helicopter configuration used in this study is not representative of an optimal semi-rigid rotor helicopter design. For example, typical helicopter configurations which are susceptible to mast bumping, feature adapted vertical offsets of main and tail rotor and incorporate underslung in the rotor hub to minimize the lead-lag loads and the resulting oscillations. Therefore, the presented results partly exaggerate the effects. Nevertheless, this study established the basic knowledge and experience required for performing quantitative analyses and implementing measures to mitigate mast bumping risks in real-world scenarios.

Author contact:
Philipp Kunze Philipp.Kunze@dlr.de
Christoph Keßler Christoph.Kessler@dlr.de
Klausdieter Pahlke Klausdieter.Pahlke@dlr.de

ACKNOWLEDGMENTS

The authors would like to thank Wolfgang von Grünhagen for insightful discussions on helicopter flight mechanics and rotor dynamics. Furthermore, the MAECOsim® development team at the DLR is acknowledged for making the presented simulations possible.

REFERENCES

1. Jenkins, V., and O´Hare, M., "Mast Bumping in Huey and Cobra Helicopters," Case Program C15-88-800.0,

Harvard Kennedy School of Government, Cambridge, MA, USA, 1988.

2. Center, U. A. S., "Mast Bumping – Causes and Prevention," Educational Video TF 46-6229, U.S. Army Air Mobility Research and Development Laboratory, 1980.

3. Dooley, L., "Rotor Blade Flapping Criteria Investigation," Technical Report USAAMRDL TR 76-33, U.S. Army Air Mobility Research and Development Laboratory, Fort Eustis, Virginia, USA, December 1976.

4. Dooley, L., "Effect of Operational Envelope Limits on Teetering Rotor Flapping," Technical Report USAAMRDL TR 78-9, U.S. Army Air Mobility Research and Development Laboratory, Fort Eustis, Virginia, USA, July 1978.

5. Sarathy, S., Schrage, D., and Losier, P., "An Investigation of Excessive Blade Flapping in the Robinson R22 Helicopter," 53rd Annual Forum of the American Helicopter Society, Virginia Beach, Virginia, USA, April 1997.

6. Sridharan, A., Chopra, I., and Turnour, S., "Mast Bumping Simulation and Mitigation Analysis for Teetering Rotor Systems," AHS International Technical Meeting Aeromechanics Design for Transformative Vertical Flight Forum, San Francisco, California, USA, January 2018.

7. Robinson, J., Collins, K., and Mavris, D., "Development of a Comprehensive Rotorcraft Model to Study the Susceptibility of Teetering Rotors to Mast Bumping Accidents," Vertical Flight Society 75th Annual Forum & Technology Display, Philadelphia, Pennsylvania, USA, May 2019. DOI: 10.4050/F-0075-2019-14720.

8. Hall, J., II, R. F., Hammerschmidt, J., Goglia, J., and Jr., G. B., "Special Investigation Report – Robinson Helicopter Company R22 Loss of Main Rotor Control Accidents," Technical Report NTSB/SIR-96/03, National Transportation Safety Board, Washington, D.C., USA, April 1996.

9. Hofmann, J., Weiß, F., and Mindt, M., "A New Approach to Comprehensive Rotorcraft Aeromechanics Simulation," 77th Annual Vertical Flight Society Forum, Palm Beach, Florida, USA, May 2021.

10. Mindt, M., "Merging an Analytical Aerodynamic Model for Helicopter Applications with a State-Space Formulation for Unsteady Airfoil Behavior," Deutscher Luft- und Raumfahrtkongress 2018, Friedrichshafen, Germany, September 2018.

11. Hofmann, J., and Röhrig-Zöllner, M., "Coupling Rotor Dynamics With a Parallel Airflow Simulation," ISC High Performance 2016 (ISC2016), Frankfurt, Germany, June 2016.

12. Seidel, C., and Peters, D., "How Big is a Lock Number?" *Journal of the American Helicopter Society*, Vol. 66, (1), January 2021. DOI: 10.4050/JAHS.66.012001.

13. Tischler, M., and Remple, R., *Aircraft and Rotorcraft System Identification: Engineering Methods with Flight-Test Examples*, AIAA, August 2006. DOI: 10.2514/4.861352.

14. Robinson Helicopter Company, "Low-G Pushovers – Extremely Dangerous," Safety Notice SN-11, Robinson Helicopter Company, Torrance, CA, USA, October 1988.

15. Robinson Helicopter Company, "High Winds or Turbulence," Safety Notice SN-32 (revised), Robinson Helicopter Company, Torrance, CA, USA, October 2020.

16. Head, E., "How Robinson Helicopter Arrived at its New Tail Design," Vertical, online: verticalmag.com, posted: 2023-09-21, visited: 2025-02-25.